Check for updates

Facile Chemical Route to Prepare Water Soluble Epitaxial Sr$_3$Al$_2$O$_6$ Sacrificial Layers for Free-Standing Oxides

*Pol Salles, Ivan Caño, Roger Guzman, Camilla Dore, Agustín Mihi, Wu Zhou, and Mariona Coll**

The growth of epitaxial complex oxides has been essentially limited to specific substrates that can induce epitaxial growth and stand high temperature thermal treatments. These restrictions hinder the opportunity to manipulate and integrate such materials into new artificial heterostructures including the use of polymeric and silicon substrates and study emergent phenomena for novel applications. To tackle this bottleneck, herein, a facile chemical route to prepare water-soluble epitaxial Sr$_3$Al$_2$O$_6$ thin films to be used as sacrificial layer for future free-standing epitaxial complex oxide manipulation is described. Two solution processes are put forward based on metal nitrate and metalorganic precursors to prepare dense, homogeneous and epitaxial Sr$_3$Al$_2$O$_6$ thin films that can be easily etched by milli-Q water. Moreover, as a proof of concept, a basic heterostructure consisting of Al$_2$O$_3$/Sr$_3$Al$_2$O$_6$ on SrTiO$_3$ is fabricated to subsequently exfoliate the Al$_2$O$_3$ thin film and transfer it to a polymer substrate. This is a robust chemical and low-cost methodology that could be adopted to prepare a wide variety of thin films to fabricate artificial heterostructures to go beyond the traditional electronic, spintronic, and energy storage and conversion devices.

1. Introduction

Complex oxides are of great interest for their rich variety of chemical and physical properties including magnetism, ferroelectricity, multiferroicity, catalytic behavior, and superconductivity.[1] Up to date, the preparation of crystalline complex oxide thin films has been mainly limited on substrates that can stand high temperature thermal treatments and on single crystal substrates when epitaxial growth is pursued. These requirements dramatically limit their applicability excluding the possibility to prepare many artificial multilayered architectures to investigate emergent phenomena that arise in thin films and at their interfaces,[2] as well as the fabrication of flexible devices and monolithic integration into silicon.[3–5] Many efforts have been devoted to develop procedures to detach the functional oxide film from the growth substrate in order to be able to freely manipulate it. They include mechanical exfoliation,[6] dry etching,[7,8] and wet-chemical etching.[9,10] Among the chemical etching procedures, the use of a sacrificial layer, which is incorporated between the substrate and the functional oxide, appears as a fast and relatively low-cost process. For this approach to be successful, the sacrificial layer should transfer the epitaxy from the substrate to the desired oxide, stand the deposition process of the functional oxide and be selectively removed by a chemical treatment, which allows to retrieve the original single-crystal substrate. (La,Sr)MnO$_3$ has been proved effective to be selectively etched by an acid blend allowing the transfer of single epitaxial Pb(Zr,Ti)O$_3$ layers[11] and more complex architectures such as SrRuO$_3$/Pb(Zr,Ti)O$_3$/SrRuO$_3$.[12] Recently, the use of water-soluble Sr$_3$Al$_2$O$_6$ (SAO) sacrificial layer enlarged the family of free-standing epitaxial perovskite oxide layers (SrTiO$_3$, BiFeO$_3$, BaTiO$_3$)[13–15] and multilayers (SrTiO$_3$/(La,Sr)MnO$_3$)[16] that can be manipulated opening a whole new world of opportunities.[5,10,17] The deposition techniques to prepare such structures is also a key factor to be considered not only for film quality but also for process scalability. While high vacuum deposition techniques such as molecular beam epitaxy and pulsed laser deposition are well established techniques to produce high quality films,[1,18–20] alternate procedures that can deliver low-cost production such as solution processing and atomic layer deposition are gaining interest.[21,22]

Chemical solution deposition (CSD) is considered a mature technique for the preparation of oxide films. The synthesis of ternary and quaternary oxides is not a trivial task but the pioneering work done in ferroelectric lead zirconate titanate inspired many researchers to extend it to other compositions and broaden the application fields.[23,24] Nonetheless, there is still a myriad of compositions to be explored, including SAO,

P. Salles, I. Caño, C. Dore, Dr. A. Mihi, Dr. M. Coll
ICMAB-CSIC
Campus UAB 08193, Bellaterra, Barcelona, Spain
E-mail: mcoll@icmab.es
Dr. R. Guzman, Prof. W. Zhou
School of Physical Sciences and CAS Key Laboratory of Vacuum Physics
University of Chinese Academy of Sciences
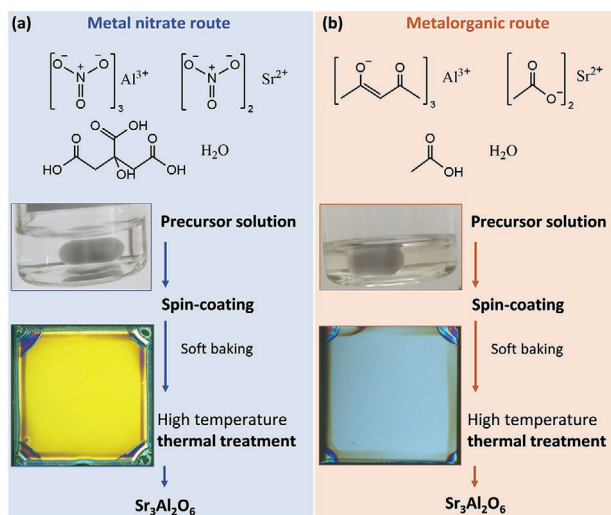Beijing 100049, China

Figure 1. Solution processing scheme to prepare SAO thin films from a) metal nitrate route and b) metalorganic route.

which brings new synthetic challenges that requires a better understanding on the role of the solution-precursor chemistry on the film properties.

Here we will tackle the synthesis of SAO prioritizing the use of environmentally benign solvents assessing the influence of precursor chemistry on the film structure and morphology. Among the plethora of salt precursors suitable for the synthesis of metal oxides, metal nitrate and metalorganic precursors are here examined. Although these are two popular routes to prepare metal-oxides,[21,25] a procedure to prepare epitaxial SAO is unexplored. We demonstrate that using metal nitrate and metalorganic precursors, homogeneous solutions can be stabilized and spin-coated on single crystal substrates. Upon high thermal treatment optimization, epitaxial SAO is successfully obtained by both routes. Etching selectivity using common solvents such as water, methanol, acetone, and acetic acid is here presented. Ultimately, to test the viability of SAO as sacrificial layer, thin films of amorphous Al_2O_3 are deposited by atomic layer deposition (ALD) on SAO and transferred to a polymeric support.

2. Results and Discussion

The development of the synthesis of SAO by CSD encompassed three main steps: stabilization of the precursor solution, homogeneous deposition by spin-coating and thermal treatment to convert the precursor gel to pure-phase and epitaxial films, as will be discussed in detail below, see **Figure 1**.

2.1. Solution Chemistry

Metal nitrate precursors are often soluble in water, they have a relatively low decomposition temperature and the high-volatility of the decomposition products minimizes the presence of residual contaminants in the final film.[25] In this work, SAO films prepared from the metal nitrate route were carried out by mixing aluminum nitrate ($Al(NO_3)_3$) and strontium nitrate

$(Sr(NO_3)_2)$ in water. The chelating agent citric acid (CA) was employed to minimize hydrolysis and condensation reactions and ensure the $SrTiO_3$ (STO) substrate wettability to obtain an homogeneous gel after spin-coating.

On the other hand, the use of mixed metalorganic compounds (carboxylates and alkoxides or β-diketonates) is a common route for the preparation of perovskite oxides and there is a plethora of commercially available precursors. Nonetheless, finding a suitable solvent for a system that includes several metalorganic compounds might be an arduous task.[26] The combination of strontium acetate ($Sr(CH_3COO)_2$) and aluminum acetylacetonate ($Al(CH_3COCH=C(O)CH_3)_3$) enables the preparation of a relatively simple solution by being dissolved in acetic acid. To improve solution stability and avoid acetylacetonate precipitation, 0–10% of water was added.[26,27] However, the precursor solution ages after few days revealed by the precipitation of aluminum acetylacetonate, see Figure S1, Supporting Information.

To ensure a controlled transformation process from the precursor salts to the formation of pure phase SAO, thermal decomposition of both precursor solutions need to be investigated.

2.2. Thermal Decomposition and Phase Formation

The thermogravimetric analysis (TGA) of the derived gel from the metal nitrate route is shown in **Figure 2**a–c. The TGA and derivative (DTG) curves show four-step mass losses, Figure 2a,b. The first step between 100 °C and 270 °C is the most pronounced with a mass loss of 53%, followed by a subtle but long second step between 270 and 550 °C with a 20% mass loss. The third step occurs between 550 and 670 °C (5%) and the last one between 740 and 930 °C (5%). Along with the first and second mass loss, several exothermic peaks can be seen in the differential scanning calorimetry (DSC) curve (Figure 2c). According to the thermogravimetric analysis reported for the individual metal nitrates and CA,[28,29] simultaneous phenomena can take place in this range of temperature. It involves the CA decomposition through intermediates such as aconitic acid,[30] the dehydration and condensation of $Al(NO_3)_3$, and the elimination of NO_x and CO_2 gases as reaction products. The third and fourth mass loss could be related to the decomposition of $Sr(NO_3)_2$ through the formation of $SrCO_3$ and the release of gases such as H_2O, NO_x, and CO_2.[31] From 740 to 930 °C, final decomposition of the intermediates, elimination of gases, probably CO_2 and O_2,[32] and crystallization of $Sr_3Al_2O_6$ may occur,[33] consistent with the large endothermic peak present in the DSC curve. Note the fact that our starting gel contains a mixture of nitrates and organics (CA), therefore, the formation of intermediates and their decomposition can moderately differ from that reported for the respective nitrates and CA. Mass spectroscopy coupled to TGA could supply additional information on the specific decomposition products of our gels, however, this detailed study is out of the scope of this work. Nonetheless, the TGA study here presented is valuable to define a tentative thermal profile consisting of a soft baking at 120 °C in air to tackle the major mass loss and then a high temperature treatment at temperatures >700 °C to promote the SAO crystallization.

The thermal decomposition analysis for the acetate and acetylacetonate precursors is shown in Figure 2d–f. Here, three
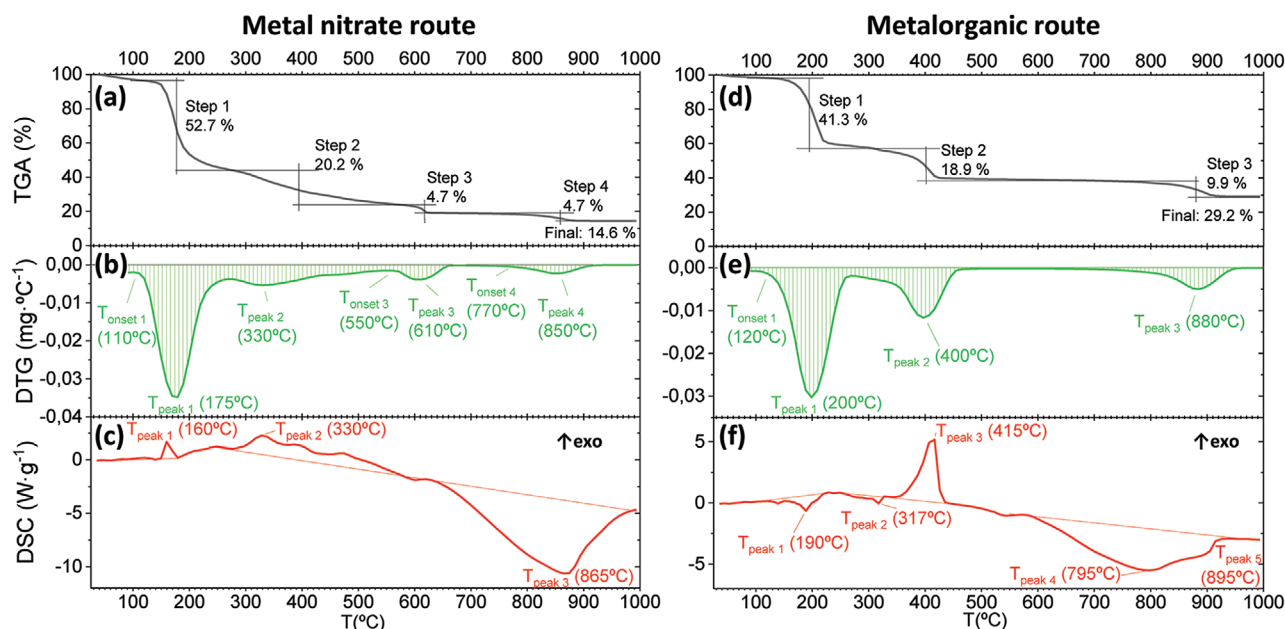
Figure 2. Thermal analysis of SAO precursor solutions. The metal nitrate solution analysis on the left side, with the corresponding a) thermogravimetric analysis, TGA, and its derivative b) DTG and c) the differential scanning calorimetry, DSC. The metalorganic route on the right, with its d) TGA, e) DTG, and f) DSC.

mass loss steps are identified. From 100 to 270 °C (41%), from 270 to 480 °C (19%) and from 710 to 960 °C (10%). The first mass loss mainly involves two-three endothermic peaks. At this temperature range, dehydration of the two reagents followed by melting and decomposition of $Al(CH_3COCH=C(O)CH_3)_3$ to Al_2O_3 can occur.[34,35] A small endothermic peak and a sharp exothermic peak occurs in the second step of mass loss that could be assigned to the melting of $Sr(CH_3CO_2)_2$ and conversion to carbonate, $SrCO_3$, respectively, with the release of CO_2, H_2O, and acetone.[32,36] The final decomposition process occurs between 800–950 °C, where carbonates are expected to decompose to the oxide forming the $Sr_3Al_2O_6$ phase with the release of CO_2. Note that the decomposition of the metalorganic precursors takes place below 500 °C whereas for the metal nitrate route is enlarged to higher temperature (≈700 °C) in well agreement with previous reports on the synthesis of complex oxides from acetates versus nitrates.[32] Based on that, the thermal profile defined for the metalorganic route consists of a two-step soft-baking (5 min at 150 °C and 5 min at 230 °C in air) and then expose the sample at high temperatures >700 °C.

According to the above thermal decomposition analysis, fine tuning of the processing parameters have been carried out: temperature (700–900 °C), time (10–90 min), heating/cooling ramps (5–660 °C min^{-1}) in oxygen atmosphere, and the structural evolution of the films has been investigated by X-ray diffraction (XRD), see Figure S2, Supporting Information. **Figure 3**a shows a representative XRD θ–2θ scan of the optimized 70 nm film from the metal nitrate route. The presence of Bragg reflections at 22.5°, 45.8°, and 71.7° appearing as a shoulder of the (00l) STO Bragg reflections (see inset Figure 3a), can be assigned to the epitaxial growth of SAO on STO. Moreover, no crystalline secondary phases are detected in the analyzed θ–2θ range. The XRD pole figure measurements around the (110)

STO and (660) SAO reflections reveal a cube on cube growth with fourfold symmetry, see Figure S3, Supporting Information. The crystalline quality of the SAO film was further characterized by XRD rocking curve (ω) around the (008) SAO reflection with a full width at half maximum (FWHM) value of 0.13° (FWHM = 0.02° for STO), Figure 3b. In-plane XRD ϕ-scan measurement around the (660) SAO results in FWHM values of 0.71° (FWHM = 0.10° for STO), Figure 3c, confirming the biaxial texture. Reported texture analysis for physical deposited SAO films, molecular beam epitaxy (MBE), show rocking curve FWHM values slightly smaller, that is, FWHM = 0.015° (FWHM= 0.013° for STO).[20] Cross-sectional Z-contrast high angle annular dark field (HAADF) using scanning transmission electron microscopy (STEM), Figure 3d,e, further confirms the epitaxial growth of SAO film on the STO (001) substrate. The HAADF-STEM images show high crystal quality and sharp interface. The typical rhombic motifs of the Sr atoms in $Sr_3Al_2O_6$ observed in higher resolution images (Figure 3c) confirms the growth of the $Sr_3Al_2O_6$ phase viewed along the [001].

SAO films prepared from the metalorganic route also led to highly epitaxial films showing sharp and intense (00l) Bragg reflections, with out-of-plane and in-plane texture of $\Delta\omega = 0.09°$ and $\Delta\phi = 0.84°$, respectively, see Figure S4, Supporting Information. Note that the intensity of the SAO peaks is higher than the films from the metal nitrate route because the films are thicker, 120 nm, in good agreement with a more viscous precursor solution (8.8 mPa·s versus 4.1 mPa·s).

Both routes lead to a homogeneous and crack free film, see optical microscope images from Figure 1. Further surface morphology analysis carried out by atomic force microscopy (AFM) reveals a granular surface with an root mean square (rms) roughness of 2.5 and 5.3 nm for the metal nitrate and metalorganic routes, respectively, Figure S5, Supporting Information.
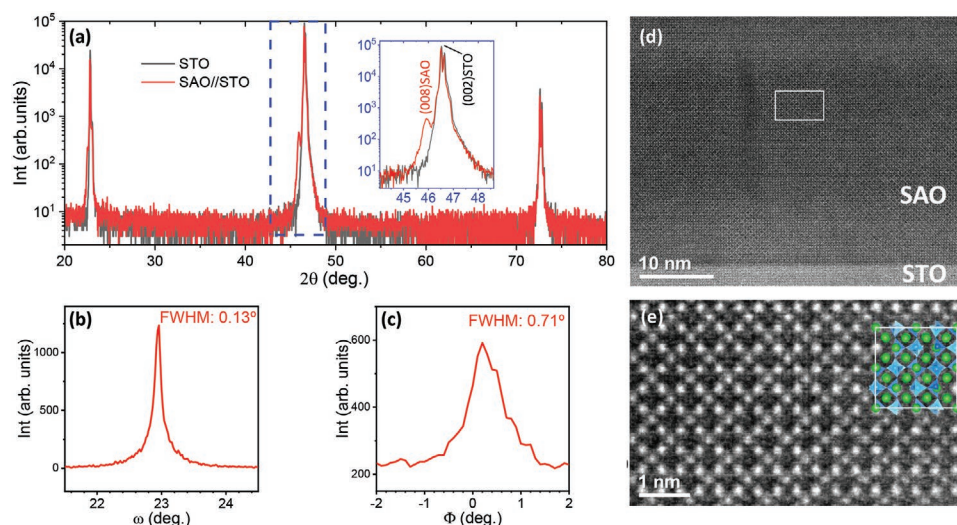
ADVANCED
SCIENCE NEWS
www.advancedsciencenews.com

ADVANCED
MATERIALS
INTERFACES
www.advmatinterfaces.de

Figure 3. SAO thin film structural characterization. a) XRD θ–2θ scan of a SAO thin film on STO substrate prepared from the metal nitrate route compared to bare STO substrate. Inset corresponding to the θ–2θ range of the (008) SAO peak and (002) STO peak. b) Rocking curve around the (008) SAO reflection and c) Phi-scan around the (660) SAO reflection. d) Z-contrast HAADF-STEM cross-section of SAO//STO interface and e) Higher magnification Z-contrast image of the SAO film showing crystallographic order at the atomic level. A single $Sr_3Al_2O_6$ unit cell atomic structure is overlaid, where green atoms are Sr and blue atoms Al. Oxygen atoms are omitted for clarity.

Note that MBE and pulsed laser deposition films of thickness ranging from 8 unit cells to 20 nm show a step-and-terrace surface morphology (with rms <0.7 nm), replicating the STO surface.[15,16,20] Importantly, SAO exposure to ambient moisture can severely degrade the surface morphology.

2.3. Etching of Sacrificial Layer

The purpose to study the effect of solvents on the integrity of SAO is twofold. First, to identify the solvents that effectively remove SAO and second, to investigate which solvents do not degrade the SAO being of interest if the heterostructure is aimed to be prepared from all-solution methodology.

It has been investigated four different common solvents used in CSD: acetic acid/methoxyethanol blend, methanol, acetone, and water. Figure S6, Supporting Information shows the optical micrograph images of the samples exposed 1 min to the different solvents and compared to an as-prepared SAO. The results indicate that the SAO thin film is not affected by the immersion in the solvent blend acetic acid/methoxyethanol. On the other hand, its immersion in methanol and acetone deteriorates the sample. Finally, the use of milli-Q water completely etches the SAO film in a few seconds, proving its effectiveness as etching solvent, in well agreement with previous studies performed on high-vacuum deposited films.[9,13,16,37] Importantly, the latter STO substrates can be recycled and used for subsequent film growth studies.

2.4. Free-Standing Al_2O_3 Films

The capability of SAO to act as a sacrificial layer for transferring free-standing oxides is here examined by depositing a 40 nm Al_2O_3 thin film by ALD on SAO//STO and transferring it to a polydimethylsiloxane (PDMS) support. Atomic layer deposition has been chosen as the deposition technique for Al_2O_3, using ozone as co-reactant, stimulated by its low-temperature and chemical gas-phase characteristics, which is expected to minimize interface diffusion, but also for the rapid pickup of the technique in industry which would facilitate the integration of this approach in already existing industrial processes.[38] From AFM analysis it has been investigated the surface morphology of the as-deposited Al_2O_3 on SAO//STO and compared to the bare SAO//STO. Both samples show smooth and continuous surface defined by fine grain size resulting in an rms of 2.5 nm, **Figure 4**. Therefore, the deposition of Al_2O_3 does not introduce surface defects on SAO thanks to the low-temperature and conformal coating nature of the ALD. Note that when Al_2O_3 is deposited on freshly cleaned STO substrates, the typical step-and-terrace morphology is identified, Figure S7, Supporting Information.

The deposition and exfoliation process followed in this work is schematized in **Figure 5**.

First, the SAO thin film is prepared by CSD on a STO substrate following the metalorganic route described above. Then, the Al_2O_3 film is deposited on the SAO//STO whose edges have been previously covered by tape to assure that the can penetrate and etch the SAO film after the Al_2O_3 coating, Figure 5c,d.
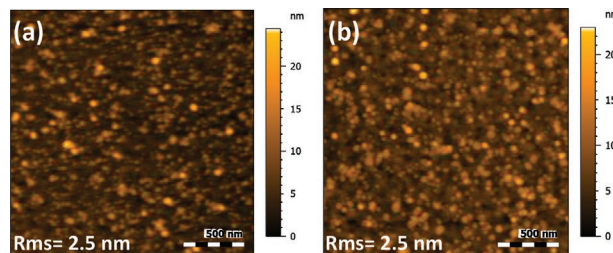

Figure 4. 2 μm × 2 μm AFM topographic images of a) SAO//STO film and b) 40 nm ALD-Al_2O_3/SAO//STO.
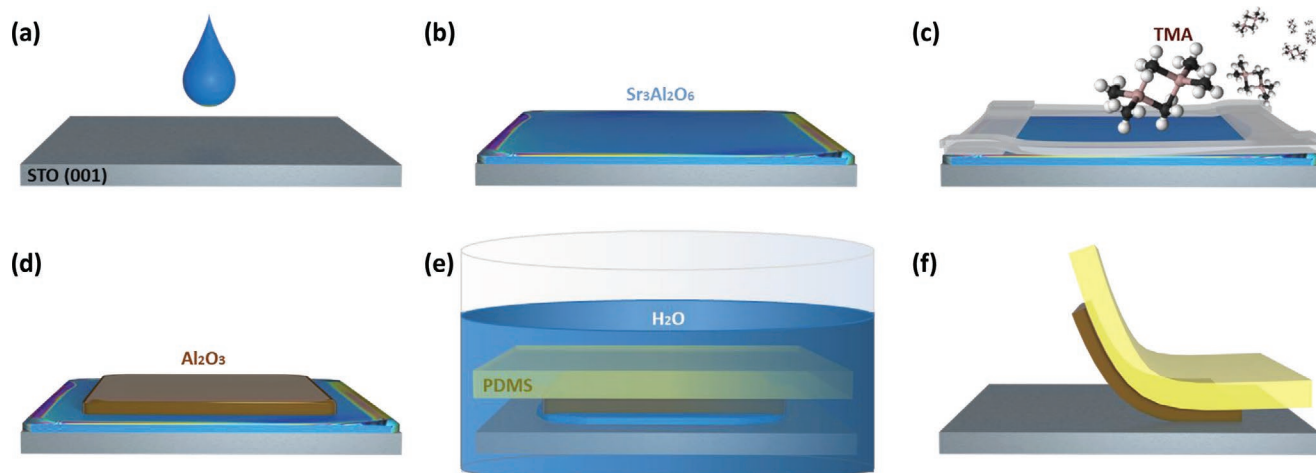
Figure 5. Scheme of the process followed to obtain Al_2O_3 films on a polymer support. a) spin-coating of SAO solution on STO substrate and processing to obtain b) SAO epitaxial film; c) atomic layer deposition of Al_2O_3 on SAO//STO, with edges masked, to obtain d) Al_2O_3 film; e) immersion in milli-Q water of PDMS supported Al_2O_3/SAO//STO system for SAO etching; f) PDMS/Al_2O_3 detachment from STO substrate.

Next, the PDMS is adhered to the heterostructure and the system is immersed in milli-Q water where the etching of SAO takes places, Figure 5e. Finally, the PDMS/Al_2O_3 can be exfoliated from the STO, Figure 5f.

Following this procedure it has been possible to transfer a continuous 0.4×0.4 cm^2 piece of 40 nm of Al_2O_3 on PDMS, see **Figure 6**a. This PDMS/Al_2O_3 architecture has been subsequently characterized by scanning eletron microscopy-energy-dispersive X-ray spectroscopy (SEM-EDX) upon transferred on a conductive carbon tape identifying the presence of aluminum on the transferred piece, Figure 6b,c.

Therefore, the combination of CSD-SAO and ALD-Al_2O_3 allowed to demonstrate the potential of CSD-SAO as sacrificial layer to transfer oxide films opening the door to future studies on freestanding epitaxial oxides by an all-chemical route.

3. Conclusions

In this study we have developed a new procedure to prepare epitaxial $Sr_3Al_2O_6$ thin films on STO by solution deposition. Metal nitrate and metalorganic precursors can be used as precursor sources upon optimization of film decomposition and crystallization. Etching of $Sr_3Al_2O_6$ is effective with water,

whereas methanol and acetone partially degrades the film. Finally, free-standing ALD-Al_2O_3 films can be obtained from SAO//STO and transferred to a PDMS stamp under mild conditions. Therefore, we present a low-cost, scalable platform that can enable further exploration of the preparation of self-supporting (epitaxial) oxides, offering another alternative to detach the synthesis of oxides from the rigid lattice matched substrate. It is envisaged many new opportunities to prepare artificial oxide heterostructures and devices offering a whole new dimension for microelectronics, photovoltaics, spintronics, and optoelectronics.

4. Experimental Section

Thin Film Preparation: $Sr_3Al_2O_6$ thin films were prepared by chemical solution deposition using two different routes named by the chemistry of the precursors, metal nitrate and metalorganic route. For the metal nitrate route, stoichiometric amounts of strontium nitrate, $Sr(NO_3)_2$ (>99%) and hydrated aluminum nitrate, $Al(NO_3)_3 \cdot 9H_2O$ (>98%) were dissolved as purchased in milli-Q water with citric acid (CA), $C_6H_8O_7$ (>99%). The precursor solution was stirred for 3 h at 90 °C in a reflux condenser to obtain a 0.25 M solution. The molar ratio of CA to total metal cations CA:M was 2:1, obtaining a viscosity of 4.1 mPa·s. The solution was filtered with a PTFE hydrophilic filter of 0.45 µm pore size previous to deposition. For the metalorganic route, stoichiometric amounts of strontium acetate, $Sr(C_2H_3O_2)_2$, and aluminum
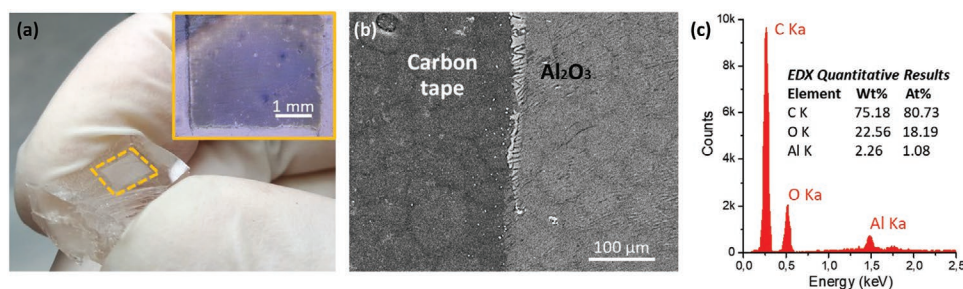

Figure 6. Transferring of Al_2O_3 films. a) Exfoliated ALD-Al_2O_3 film on a PDMS support. Inset: magnified image of the transferred Al_2O_3 film. b) SEM and c) EDX of Al_2O_3 film transferred from the PDMS support to a carbon tape.

**ADVANCED
SCIENCE NEWS**

www.advancedsciencenews.com

**ADVANCED
MATERIALS
INTERFACES**

www.advmatinterfaces.de

acetylacetonate, $Al(C_5H_7O_2)_3$ (>99%), were dissolved in a solvent blend of acetic acid (>99.8%) and milli-Q water to obtain a 0.25 м solution. The precursor solution was stirred for 3 h at 60 °C. The percentage of water in solution was varied between 0–10 %, obtaining a viscosity of 8.8 mPa·s when 5 % water is used. The solutions were filtered with a PTFE filter of 0.22 μm pore size.

The solutions were spin-coated by disposing 15 μL on a 5×5 mm^2 monocrystalline $SrTiO_3$ (STO) (001) substrate. For the metal nitrate route, the STO substrate was exposed to a UV–ozone pre-treatment for 5 min to improve wettability. The samples were spun at 6000 rpm for 30 s and then exposed to a soft baking. The nitrate samples at 120 °C for 10 min and the metalorganic 5 min at 150 °C + 5 min at 230 °C (according to the thermogravimetrical analysis, Figure 2). Finally, the samples were introduced in a tubular furnace, where annealing temperature (700–900 °C), time at that temperature (10–90 min) and heating/cooling rate (5–25 °C min^{-1} - flash heating (660 °C min^{-1})) were optimized, Figure S3, Supporting Information. The optimal conditions were a heating ramp of 25 °C min^{-1} from room temperature to 800–900 °C and cooled down at 25 °C min^{-1}, all under 0.6 l·min^{-1} O_2 flow. Annealing time was optimized according to film thickness. The samples, specially those prepared from the metal nitrate route, are very sensitive to moisture. Solution deposition process and sample manipulation until it is exposed to soft backing (230 °C) should be handled in relative humidity <30%.

The transfer of the deposited Al_2O_3 thin film was done using polydimethyl siloxane PDMS Sylgard 186 as support. Both the PDMS support and the heterostructure $Al_2O_3/SAO//STO$ were exposed to a UV–ozone treatment for 5 min to improve adhesion, before mild pressing them, and then the structure was immersed in milli-Q water for etching. Finally, PDMS and STO were mechanically separated, obtaining on one side the PDMS with the Al_2O_3 thin film on it and, on the other side, a clean STO. After recovering the STO substrate, it was further treated for a better recycling. First, 10 min sonication in H_2O was used to remove any remaining traces, and then 30 s immersion in buffered HF solution (30%) and post-annealing for 1 h at 950 °C was proceeded to recover the terrace-like morphology,[39] see Figure S5d, Supporting Information.

Al_2O_3 thin films have been deposited by ALD using a commercial reactor from Savannah–Cambridge Nanotech 100 in flow mode. Trimethylaluminum and ozone were alternatively pulsed/purged for 0.05 s/5 s and 0.1 s/7 s, respectively under a 20 sccm N_2 carrier gas. The reactor temperature was set at 150 °C for 400 cycles. Under these conditions, we obtained 40 nm films of amorphous Al_2O_3.

Thermogravimerical Characterization: TGA and DSC were done with a thermal analyzer METTLER TOLEDO model TGA/DSC 1 equipped with a oven HT1600 and microbalance MX5 at University of Málaga, with a range of temperatures from 30 to 1000 °C, heating rate of 10 °C·min^{-1}, and O_2 flow of 50 mL· min^{-1}. In order to carry out this study, the precursor solutions were previously dried to a gel by a rotary evaporator (R-100).

Surface Morphology Characterization: Magnified images of the thin films were taken by optical microscope (Leica S9 i and Leica DM1750 M). Surface morphology and roughness were analyzed from topographic images acquired with an AFM Keysight 5100 instrument and analyzed using Mountains Software. Surface morphology was also analyzed by SEM, together with chemical analysis by EDX, with a SEM QUANTA FEI 200 FEG-ESEM.

Structure Characterization: Phase and crystalline structure of the SAO films were studied by XRD using a Siemens Diffractometer D-5000 along a scan range of 2θ 20–80°. Texture analysis has been performed by XRD pole figure measurements using a Bruker-AXS, model D8 Advance diffractometer equipped with a bidimensional detector Vantec-500 (GADDS). Out-of-plane and in-plane texture analysis have been performed by XRD rocking curve and phi scan, respectively, using Bruker-AXS, model A25 D8 Discover diffractometer. All three diffractometers are with Cu-Kα = 1.5418 Å.

Aberration-corrected STEM imaging were performed using a Nion HERMES-100, operated at 100 kV. HAADF images were acquired using an annular detector with collection semi-angle of 92-210 mrad. Cross-sectional STEM specimens were prepared using the standard focused ion beam (FIB) lift-out process in a Thermo Fisher Scientific FIB system.

Protective amorphous carbon and thin Pt layers were applied over the region of interest before milling. To minimize the sidewall damage and sufficiently thin the specimen for electron transparency, final milling was carried out at a voltage of 5 kV. To reduce possible beam-induced structural damage on the SAO films, images were acquired with reduced beam current (10 pA) and pixel dwell time (2 μs·px^{-1})

Thickness of the SAO films was studied by profilometry on samples with a side cleaned with water, using a Profilometer P16+ from KLA Tencor. (Measurement made as an average of three consecutive scans, analysed using Mountains Software)

Supporting Information

Supporting Information is available from the Wiley Online Library or from the author.

Conflict of Interest

The authors declare no conflict of interest.

Keywords

[1] M. Coll, J. Fontcuberta, M. Althammer, M. Bibes, H. Boschker, A. Calleja, G. Cheng, M. Cuoco, R. Dittmann, B. Dkhil, I. E. Baggari, M. Fanciulli, I. Fina, E. Fortunato, C. Frontera, S. Fujita, V. Garcia, S. Goennenwein, C.-G. Granqvist, J. Grollier, R. Gross, A. Hagfeldt, G. Herranz, K. Hono, E. Houwman, M. Huijben, A. Kalaboukhov, D. Keeble, G. Koster, L. Kourkoutis, et al., *Appl. Surf. Sci.* **2019**, *482*, 1.

[2] M. Bibes, J. E. Villegas, A. Barthélémy, *Adv. Phys.* **2011**, *60*, 5.

[3] D. Dubbink, Ph.D. Thesis, University of Twente, Netherlands **2017**.

[4] S.-H. Baek, C.-B. Eom, *Acta Mater.* **2013**, *61*, 2734.

[5] W. Gao, Y. Zhu, Y. Wang, G. Yuan, J.-M. Liu, *J. Materiomics* **2020**, *6*, 1.

[6] J. Liu, Y. Feng, R. Tang, R. Zhao, J. Gao, D. Shi, H. Yang, *Adv. Electron. Mater.* **2018**, *4*, 1700522.

[7] L. P. Lee, M. J. Burns, K. Char, *Appl. Phys. Lett.* **1992**, *61*, 2706.

[8] C. K. Jeong, S. B. Cho, J. H. Han, D. Y. Park, S. Yang, K.-I. Park, J. Ryu, H. Sohn, Y.-C. Chung, K. J. Lee, *Nano Res.* **2017**, *10*, 437.

[9] Y. Zhang, C. Ma, X. Lu, M. Liu, *Mater. Horiz.* **2019**, *6*, 911.

[10] H. S. Kum, H. Lee, S. Kim, S. Lindemann, W. Kong, K. Qiao, P. Chen, J. Irwin, J. H. Lee, S. Xie, S. Subramanian, J. Shim, S.-H. Bae, C. Choi, L. Ranno, S. Seo, S. Lee, J. Bauer, H. Li, K. Lee, J. A. Robinson, C. A. Ross, D. G. Schlom, M. S. Rzchowski, C.-B. Eom, J. Kim, *Nature* **2020**, *578*, 75.

[11] S. R. Bakaul, C. R. Serrao, M. Lee, C. W. Yeung, A. Sarker, S.-L. Hsu, A. K. Yadav, L. Dedon, L. You, A. I. Khan, J. David Clarkson, C. Hu, R. Ramesh, S. Salahuddin, *Nat. Commun.* **2016**, *7*, 10547.

[12] S. R. Bakaul, C. R. Serrao, O. Lee, Z. Lu, A. Yadav, C. Carraro, R. Maboudian, R. Ramesh, S. Salahuddin, *Adv. Mater.* **2017**, *29*, 1605699.

[13] D. Ji, S. Cai, T. R. Paudel, H. Sun, C. Zhang, L. Han, Y. Wei, Y. Zang, M. Gu, Y. Zhang, W. Gao, H. Huyan, W. Guo, D. Wu, Z. Gu, E. Y. Tsymbal, P. Wang, Y. X. Pan, *Nature* **2019**, *570*, 87.

[14] R. Guo, L. You, W. Lin, A. Abdelsamie, X. Shu, G. Zhou, S. Chen, L. Liu, X. Yan, J. Wang, J. Chen, *Nat. Commun.* **2020**, *11*, 2571.

[15] K. Gu, T. Katayama, S. Yasui, A. Chikamatsu, S. Yasuhara, M. Itoh, T. Hasegawa, *Adv. Funct. Mater.* **2020**, *30*, 2001236.

[16] D. Lu, D. J. Baek, S. S. Hong, L. F. Kourkoutis, Y. Hikita, H. Y. Hwang, *Nat. Mater.* **2016**, *15*, 1255.

[17] W. Liu, H. Wang, *J. Materiomics* **2020**, *6*, 385.

[18] D. G. Schlom, *APL Mater.* **2015**, *3*, 062403.

[19] M. Brahlek, A. S. Gupta, J. Lapano, J. Roth, H.-T. Zhang, L. Zhang, R. Haislmaier, R. Engel-Herbert, *Adv. Funct. Mater.* **2018**, *28*, 1702772.

[20] H. Sun, C. Zhang, J. Song, J. Gu, T. Zhang, Y. Zang, Y. Li, Z. Gu, P. Wang, Y. Nie, *Thin Solid Films* **2020**, *697*, 137815.

[21] T. Schneller, R. Waser, M. Kosec, D. Payne, *Chemical Solution Deposition of Functional Oxide Thin Films*, Springer, Berlin **2013**.

[22] M. Coll, M. Napari, *APL Mater.* **2019**, *7*, 110901.

[23] J. M. Vila-Fungueiriño, B. Rivas-Murias, J. Rubio-Zuazo, A. Carretero-Genevrier, M. Lazzari, F. Rivadulla, *J. Mater. Chem. C* **2018**, *6*, 3834.

[24] M. Coll, J. Gàzquez, R. Huhne, B. Holzapfel, Y. Morilla, J. Garcia-Lopez, A. Pomar, F. Sandiumenge, T. Puig, X. Obradors, *J. Mater. Res.* **2009**, *24*, 1446.

[25] E. A. Cochran, K. N. Woods, D. W. Johnson, C. J. Page, S. W. Boettcher, *J. Mater. Chem. A* **2019**, *7*, 24124.

[26] D. Levy, M. Zayat, *The Sol–Gel Handbook: Synthesis, Characterization, and Applications*, Wiley, New York **2015**.

[27] A. J. C. Nixon, D. R. Eaton, *Can. J. Chem.* **1978**, *56*, 1928.

[28] M. M. Barbooti, D. A. Al-Sammerrai, *Thermochim. Acta* **1986**, *98*, 119.

[29] P. Melnikov, V. A. Nascimento, I. V. Arkhangelsky, L. Z. Zanoni Consolo, *J. Therm. Anal. Calorim.* **2013**, *111*, 543.

[30] D. Wyrzykowski, E. Hebanowska, G. Nowak-Wiczk, M. Makowski, L. Chmurzyński, *J. Therm. Anal. Calorim.* **2011**, *104*, 731.

[31] S. Culas, A. Surendran, J. Samuel, *Asian J. Chem.* **2013**, *25*, 3855.

[32] L. Pardo, J. Ricote, *Multifunctional Polycrystalline Ferroelectric Materials: Processing and Properties*, Springer, Berlin **2011**.

[33] P. Ptáček, E. Bartoníčková, J. Švec, T. Opravil, F. Šoukal, F. Frajkorová, *Ceram. Int.* **2015**, *41*, 115.

[34] Y. Duan, J. Li, X. Yang, X. M. Cao, L. Hu, Z. Y. Wang, Y. W. Liu, C. X. Wang, *J. Therm. Anal. Calorim.* **2008**, *94*, 169.

[35] T. Maruyama, S. Arai, *Appl. Phys. Lett.* **1992**, *60*, 322.

[36] B. Malič, M. Kosec, K. Smolej, S. Stavber, *J. Eur. Ceram. Soc.* **1999**, *19*, 1345.

[37] S. S. Hong, J. H. Yu, D. Lu, A. F. Marshall, Y. Hikita, Y. Cui, H. Y. Hwang, *Sci. Adv.* **2017**, *3*, eaao5173.

[38] K. Erwin, M. Bart, *NEVAC* **2020**, *58*, 2.

[39] G. Koster, B. L. Kropman, G. J. H. M. Rijnders, D. H. A. Blank, H. Rogalla, *Appl. Phys. Lett.* **1998**, *73*, 2920.